Available online at www.sciencedirect.com
ScienceDirect
Renewable Energy 32 (2007) 2291–2305
RENEWABLE ENERGY
www.elsevier.com/locate/renene

Fluid dynamics wind turbine design: Critical analysis, optimization and application of BEM theory

R. Lanzafame, M. Messina*

DIIM—Dipartimento di Ingegneria Industriale e Meccanica, Faculty of Engineering, University of Catania, Viale A. Doria, 6–95125 Catania, Italy

Received 29 August 2006; accepted 15 December 2006
Available online 20 February 2007

Abstract

A mathematical model for fluid dynamics wind turbine design (based on the blade element momentum theory) has been implemented and improved. The mathematical simulations have been compared with experimental data found in the literature. The simulation was performed for the whole wind velocity range, in on-design and off-design conditions. Several simulations were performed in order to maximize the agreement between the simulated and experimental data. Particular attention was paid to the tangential induction factor and to the models for the representation of the lift and drag coefficients. A comparison was also made between the mathematical model presented in the paper and those considered in the literature. Finally, the model was implemented to optimize rotor performance, especially at low wind velocities, which is crucial to produce power during the machine start-up phase.

Keywords: Wind power; Wind turbines; Blade element momentum theory; Fluid dynamics design

1. Introduction

The mathematical model most frequently used by scientific and industrial communities is the one based on the blade element momentum (BEM) theory [1–3,5–9,11–17]. It offers the possibility to perform fluid dynamics design of rotor blades, and to evaluate wind

*Corresponding author.
E-mail address: mmessina@diim.unict.it (M. Messina).

0960-1481/$ - see front matter © 2007 Elsevier Ltd. All rights reserved.
doi:10.1016/j.renene.2006.12.010

Nomenclature

R_1	wind rotor radius (m)
Re	Reynolds number (dimensionless)
α	angle of attack (rad)
θ	twist angle (rad)
ϕ	incoming flow direction angle (rad)
ω	angular velocity (s^{-1})
a	axial induction factor (dimensionless)
a'	tangential induction factor (dimensionless)
r	blade local radius (m)
V_0	wind velocity far up stream (m/s)
V_1	airfoil relative wind velocity (m/s)
T	rotor tangential force (N)
N	rotor normal force (N)
L	lift (N)
D	drag (N)
R	global force on the airfoil (N)
c	airfoil chord (m)
ρ	air density (kg/m^3)
C_L	lift coefficient (dimensionless)
C_D	drag coefficient (dimensionless)
N_b	number of blades
M	torque (Nm)
F	tip loss factor (dimensionless)
σ	solidity (dimensionless)
C_N	normal force coefficient (dimensionless)
C_T	tangential force coefficient (dimensionless)
p	pressure (Pa)
λ	tip speed ratio (dimensionless)
λ_r	local speed ratio (dimensionless)
a_i	C_L logarithmic polynomial coefficients
b_i	C_D logarithmic polynomial coefficients
P	power (W)
C_P	power coefficient (dimensionless)
LSR	local speed ratio (dimensionless)
TLF	tip loss factor (dimensionless)
TSR	tip speed ratio (dimensionless)
TLF	tip loss factor (dimensionless)
BEM	blade element momentum
CSU	Colorado State University
OSU	Ohio State University
DUT	Delft University Technology

turbine performance (in on-design and off-design conditions). With the implementation of this model it is possible to design the rotor, to choose the geometric characteristics of the turbine (rotor diameter, aerodynamic airfoils, chord, pitch and twist), and to evaluate the forces acting on the blades, and so the torque and the power at the rotor shaft. With this mathematical model it is also possible to evaluate turbine performance with a wide range of wind velocities.

The BEM theory is based on the Glauert propeller theory [9], modified for application to wind turbines. In recent years the BEM theory has been optimized and modified to provide increasingly accurate results. For the numerical stability of the mathematical model the greatest difficulties are represented by determination of the axial and tangential induction factors, the lack of experimental measurements on airfoil lift and drag coefficients at high angles of attack, and their three-dimensional representation. In order to take the three-dimensional representation into account, the wind tunnel experimental measurements must be modified in order to consider the radial flow along the blades (centrifugal pumping [8,18]).

2. The mathematical model

The mathematical model implemented in this work for the fluid dynamics design of a wind turbine is based on the BEM theory. By applying the momentum and angular momentum conservation equations, it is possible to obtain the forces acting on the blades, and so the torque and power at the rotor shaft.

Fig. 1 shows a cross-section of the rotor blade and the velocities relating to the airfoil. It also shows the axial and tangential induction factors (a and a') that significantly affect the real value of the velocities.

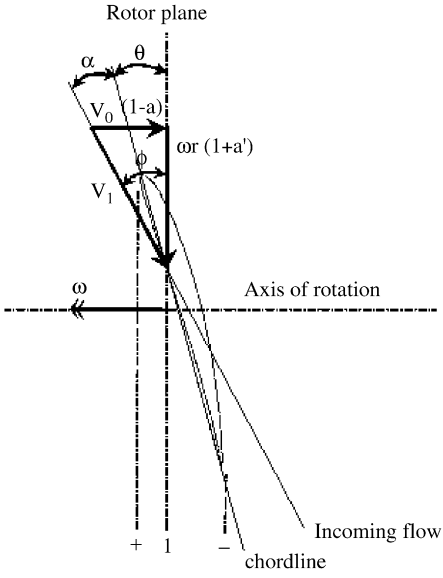

Fig. 1. Velocities relating to the airfoil.

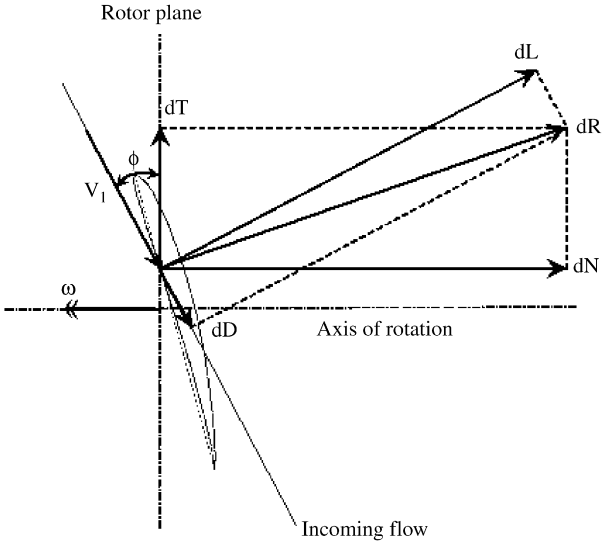

Fig. 2. Forces acting on the airfoil.

Fig. 2 shows the forces acting on the airfoil. The forces acting on the blade sector with a height of dr_1, are: dT = tangential force (tangential to the rotor disk); dN = normal force (normal to the rotor disk); dL = lift; dD = drag; and dR = resultant force.

By applying the BEM theory, it is possible to evaluate the force dN and the torque dM for each blade element, as given in Eqs. (1) and (2):

$$dN = \frac{\rho}{2}\frac{V_0^2(1-a)^2}{\sin^2\phi}N_b(C_L\cos\phi + C_D\sin\phi)c\,dr_1, \tag{1}$$

$$dM = \frac{\rho}{2}\frac{V_0(1-a)}{\sin\phi}\frac{\omega r_1(1+a')}{\cos\phi}N_b(C_L\sin\phi - C_D\cos\phi)cr_1\,dr_1. \tag{2}$$

For each aerodynamic airfoil, C_L and C_D depend on the Reynolds number and the angle of attack (see Figs. 3 and 4).

Figs. 3 and 4 give the values of the C_L and C_D coefficients for the S809 airfoil. From different wind tunnel measurements [5], Figs. 3 and 4 give the C_L and C_D coefficients for different Reynolds numbers (from 3×10^5 to 10^6), and for the typical angle of attack range (from -20° to 90°) for a wind turbine flow regime.

The torque and normal forces depend on the tangential and axial induction factors. To evaluate them it is necessary to implement the momentum and angular momentum conservation equations.

From the conservation of the momentum in the axial direction, between the far upstream section and the far downstream section, it is possible to obtain two further expressions for the force dN and the torque dM. Equalizing these two equations, with

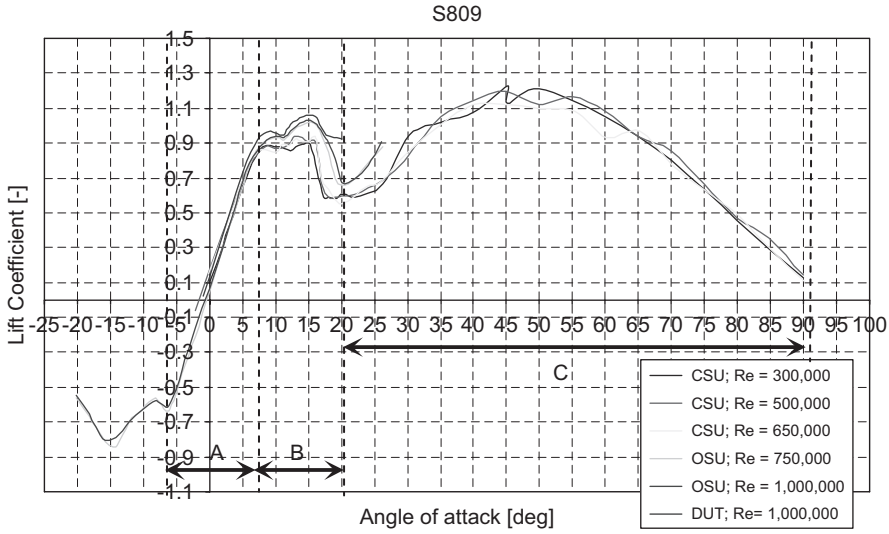

Fig. 3. Experimental lift coefficient for the S809 airfoil [5].

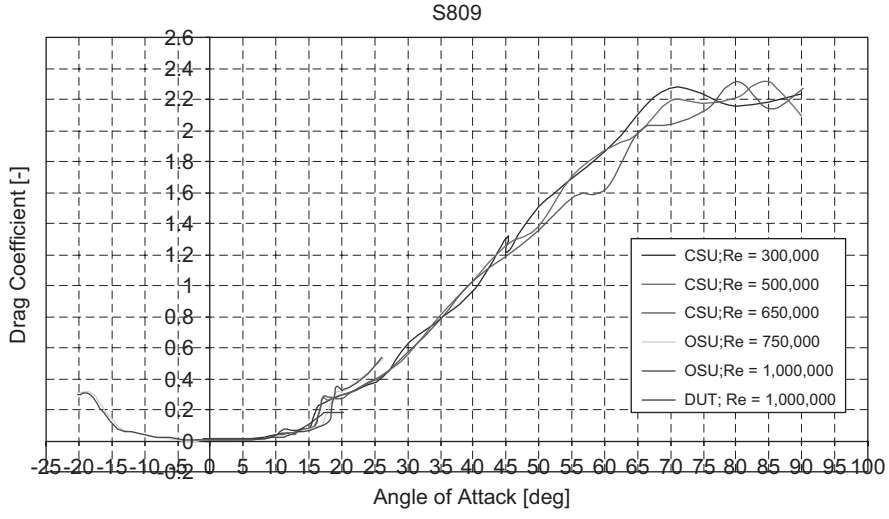

Fig. 4. Experimental drag coefficient for the S809 airfoil [5].

Eqs. (1) and (2), respectively, it is possible to obtain

$$a = \frac{1}{\frac{4F \sin^2 \phi}{\sigma(C_L \cos \phi + C_D \sin \phi)} + 1} \tag{3}$$

and

$$a' = \frac{1}{\frac{4F \sin \phi \cos \phi}{\sigma(C_L \sin \phi - C_D \cos \phi)} + 1}, \tag{4}$$

where F is the Prandtl tip loss factor, defined as [5,6]

$$F = \frac{2}{\pi} ar\cos\left[\exp\left(\frac{N_b(r_1 - R_1)}{2r_1 \sin\phi}\right)\right] \tag{5}$$

and σ is the rotor solidity, defined as

$$\sigma = \frac{cN_b}{2\pi r_1}. \tag{6}$$

3. Improvement of axial and tangential induction factors

3.1. The axial induction factor

Eq. (3) only gives reliable results for axial induction factor values between 0 and 0.4. For axial induction factors greater than 0.4 the BEM theory does not yield reliable results. Glauert [4] gave a correction for determination of the axial induction factor when $a > 0.4$, valid only for $F = 1$ (Fig. 5). If the losses at the tip of the blade are taken into account ($F < 1$), it is necessary to consider the correction (Eq. (7)) proposed by Buhl [3], and implemented in [2] (Fig. 6, with experimental data from [2]).

$$a = \frac{18F - 20 - 3\sqrt{C_N(50 - 36F) + 12F(3F - 4)}}{36F - 50}. \tag{7}$$

This correction is necessary to eliminate the numerical instability that occurs when the Glauert correction is implemented in conjunction with the presence of tip losses.

3.2. The tangential induction factor

By applying the energy equation between the upwind rotor section and the downwind section (see Fig. 1), it is possible to obtain the rotor pressure drop [5], and so the normal

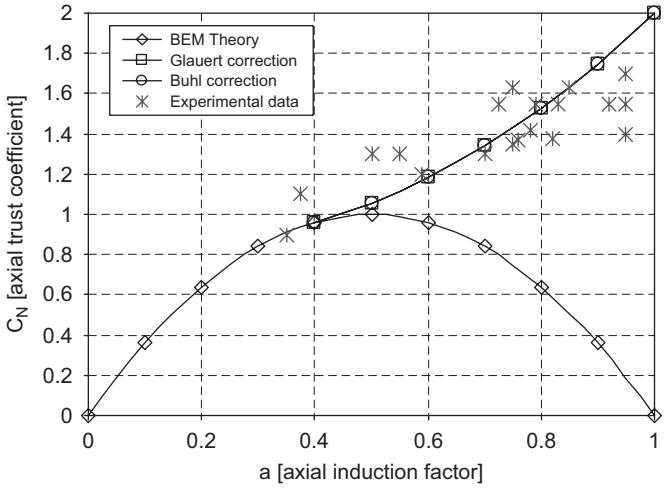

Fig. 5. $F = 1$—Glauert and Buhl corrections coincide.

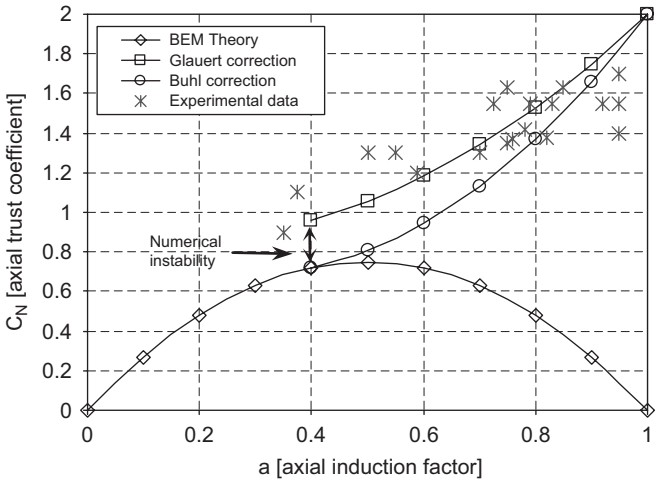

Fig. 6. $F = 0.75$—Numerical instability when $F < 1$.

force, as

$$dN = (p_1^+ - p_1^-)2\pi r_1\, dr_1 = \rho\omega^2 r_1^2 4a'(1+a')F\pi r_1\, dr_1. \tag{8}$$

In conclusion, by equalizing Eq. (8) with the normal force obtained from the BEM theory, a new expression for the tangential induction factor can easily be obtained:

$$a' = \frac{1}{2}\left(\sqrt{1+\frac{4}{\lambda_r^2}a(1-a)} - 1\right), \tag{9}$$

with λ_r defined as

$$\lambda_r = \frac{\omega r_1}{V_0}. \tag{10}$$

To verify the validity of the simulated data, the mathematical model was compared with the experimental data collected by the NREL [8] in NASA-Ames wind tunnel tests. The wind turbine is the UAE Phase VI, with two blades, twisted and with the chord variable along the blade, and with a diameter of 10 m [10]. The aerodynamic airfoil is the S809 and it is constant along the blades; the pitch is 3° and the rotational velocity is 72 r/min.

The next two figures show a comparison and the errors between the simulated and experimental data. The simulation was carried out twice, in order to verify the correctness of the tangential induction factor, evaluated with Eqs. (4) and (9).

Fig. 7 shows that the simulated torque curve is closer to experimental data when the tangential induction factor is evaluated using Eq. (9). Moreover, the tangential induction factor values evaluated with Eq. (9) are smaller than those evaluated with Eq. (4). This is due to a more accurate mathematical representation of the blade tip losses [5].

Fig. 8 shows the shaft torque relative percent error between the two mathematical simulations, and the experimental data.

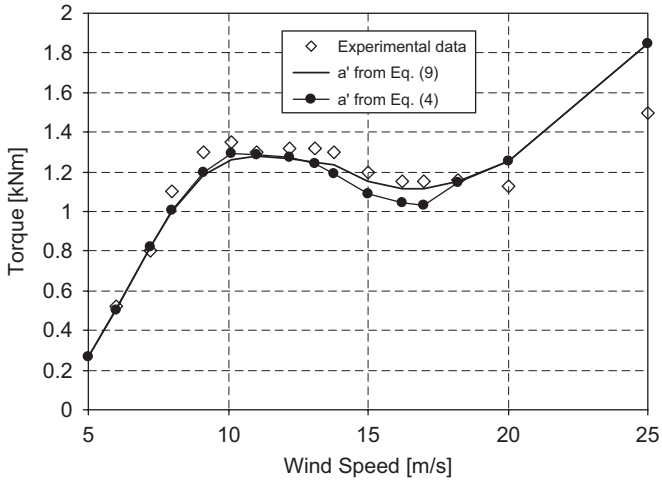

Fig. 7. Experimental and simulated shaft torques.

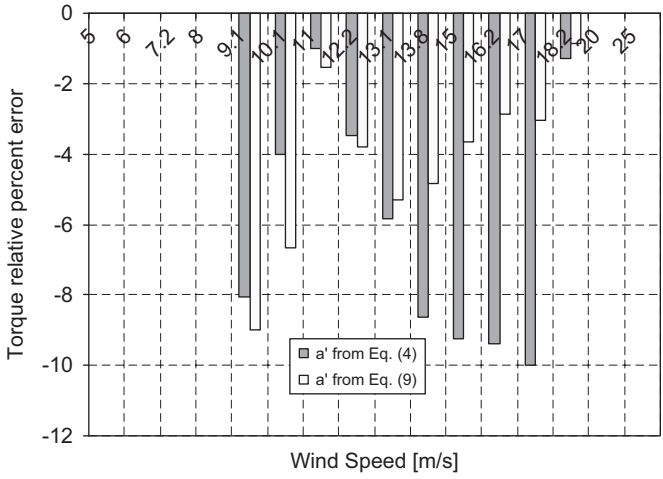

Fig. 8. Torque relative percent error between experimental and simulated data.

4. Lift and drag coefficients

The lift and drag coefficients for a given airfoil can be evaluated from wind tunnel measurements. The values given in Figs. 3 and 4 must be fitted in order to have mathematical functions for implementation in the simulation model. The flow around the airfoil is characterized by three different regimes: attached flow regime (zone A in Fig. 3); high lift, stall development regime—dynamic stall (zone B); flat plate, fully stalled regime (zone C).

To fit the experimental data on lift and drag coefficients, a fifth-order logarithmic polynomial (shifted by 10°) was implemented for the angle of attack from −6° to 20° (A and B zones), as shown in Eqs. (11) and (12).

$$C_L = \sum_{i=0}^{5} a_i [\ln(\alpha + 10)]^i, \tag{11}$$

$$C_D = \sum_{i=0}^{5} b_i [\ln(\alpha + 10)]^i. \tag{12}$$

The a_i and b_i coefficients were determined by means of the least squares root method, fitting experimental data for $Re = 10^6$.

For the "flat plate, fully stalled regime" ($20 \leqslant \alpha \leqslant 45°$) the mathematical functions of the following equations were implemented:

$$C_L = 2C_{L_{\max}} \sin \alpha \cos \alpha, \tag{13}$$

$$C_D = C_{D_{\max}} \sin^2 \alpha. \tag{14}$$

The $C_{L\max}$ and $C_{D\max}$ are shown as follows:

$$C_{L_{\max}} = C_L|_{\alpha=45°} \quad \text{and} \quad C_{D_{\max}} = C_D|_{\alpha=90°}. \tag{15}$$

5. The distribution of the lift coefficient along the blade

Fig. 9 shows the lift coefficient along the blade. In each diagram in Fig. 9, the lift coefficient distribution along the blade with different wind velocities and a pitch angle of 3° is represented by the gray rectangle. In diagrams (a) and (b), at wind speeds of 5 and 7.5 m/s, the flow is in the attached regime. In diagram (c), at a wind speed of 10 m/s, the flow is in the "high lift, stall development regime, dynamic stall". In diagram (d), at a velocity of 15 m/s, the transition from the "high lift, stall development regime, dynamic stall" to the "flat plate, fully stalled regime" occurs. In diagrams (e) and (f), at a wind speed of 20 and 25 m/s, the flow is completely in the "flat plate, fully stalled regime".

For the wind turbine considered in this work, the power production is stall controlled (see the last three charts in Fig. 9). When the wind speed goes from 10 to 25 m/s the power production is limited to about 10 kW due to a deep stall of the rotor blades. The wind speed of 25 m/s is the cutout velocity.

6. Comparison between different mathematical models

A difficult goal in the implementation of the BEM theory is the correct representation of the lift and drag coefficients. Starting from wind tunnel measurements, for a wind turbine simulation it is fundamental to take into account the radial flow along the blade. This phenomenon is absent in airfoil wind tunnel measurements, and, as widely reported in scientific literature [6,8], it causes an increment in the value of C_L, in the transition zone between the high lift, stall development regime, dynamic stall" and the "flat plate, fully stalled regime".

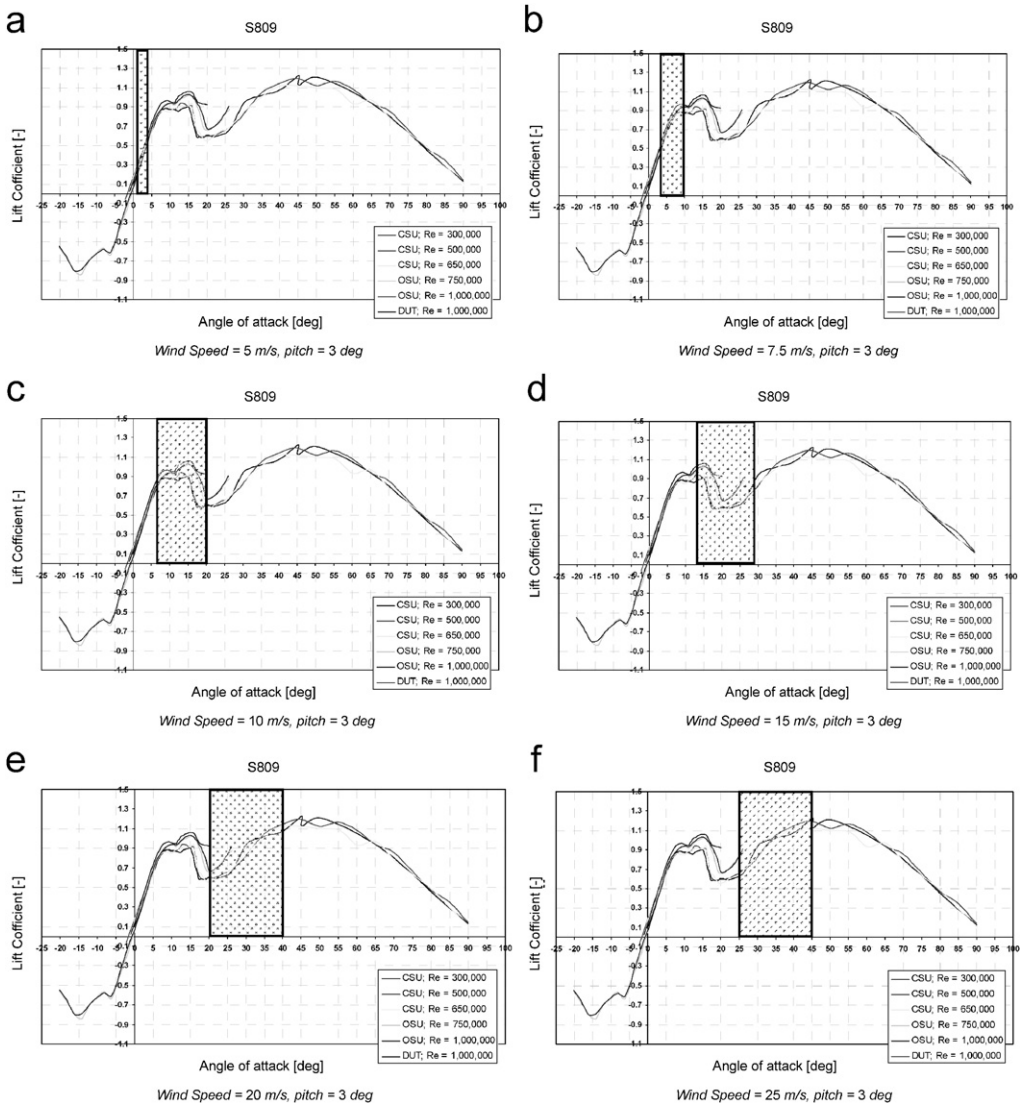

Fig. 9. Lift coefficient along the blade.

In the literature, different mathematical models are presented to describe the correct trend of C_L and C_D. Fig. 10 shows a comparison between different mathematical models representing the lift and drag coefficients.

In this work the lift and drag coefficients are represented through Eqs. (13) and (14), and a comparison was performed between the model presented here (named EOLO) and the mathematical models listed below (which also take into account losses at the tip and at the hub):

- BEM with C_L 2D: BEM Theory with C_L and C_D measured in the wind tunnel;
- Wilson and Lissman [8]: as in "BEM with C_L 2D" but with different tip loss models;

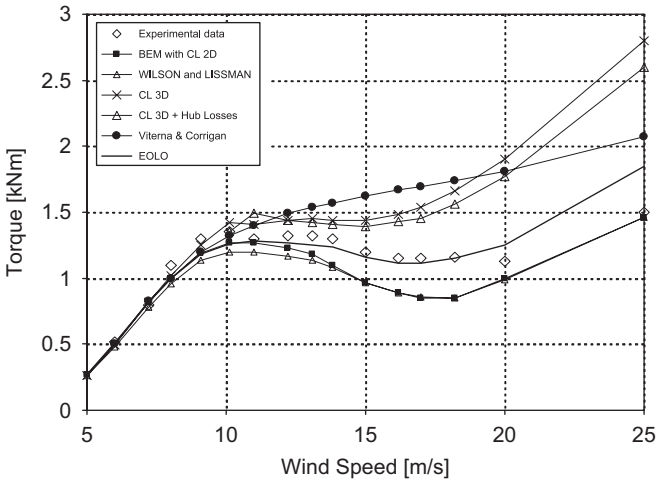

Fig. 10. Comparison between different mathematical models representing the lift and drag coefficients.

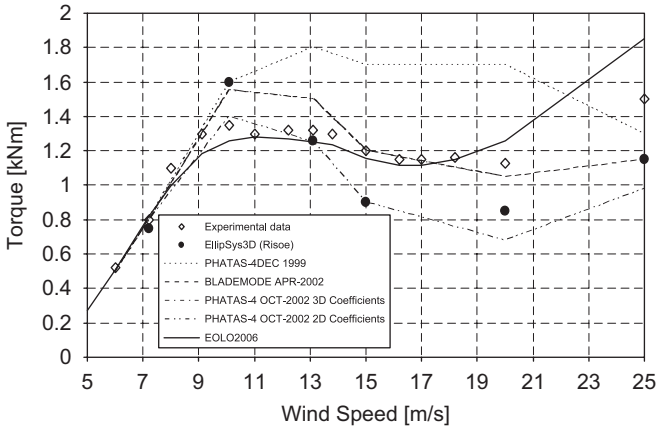

Fig. 11. Comparison between different mathematical models for the simulation of a wind turbine [8].

- C_L 3D as in [6];
- C_L 3D + hub losses;
- Viterna and Corrigan post stall model [7].

Fig. 10 gives the wind rotor shaft torque for different wind speeds. In this figure a comparison is made between different mathematical models used to describe the lift and drag coefficients. The experimental data are also included in the comparison, and the mathematical representation based on Eqs. (13) and (14) gives the best agreement between experimental and simulated data.

In the transition zone between the "high lift, stall development regime, dynamic stall" and the "flat plate, fully stalled regime", by applying the mathematical

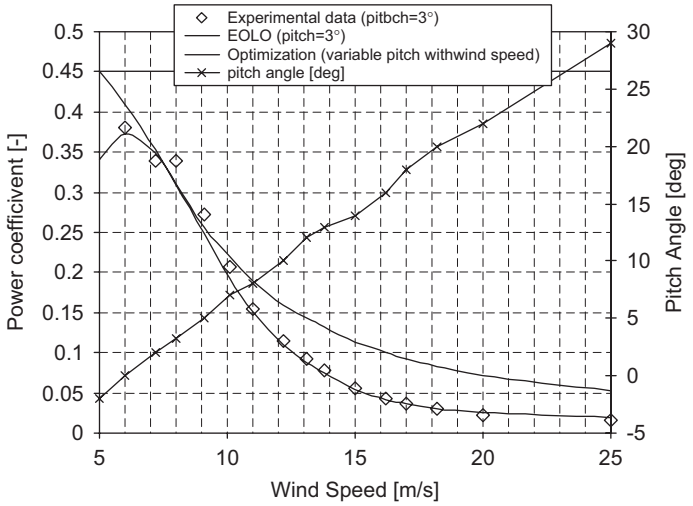

Fig. 12. Power coefficient (experimental and simulated) and pitch angle trend vs. wind speed.

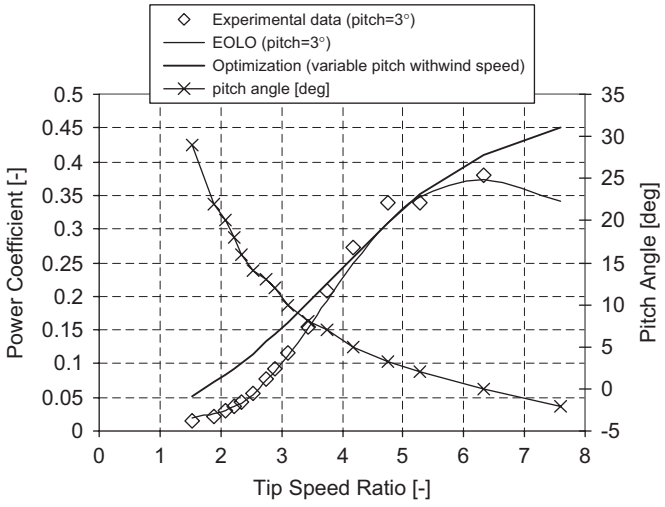

Fig. 13. Power coefficient (experimental and simulated) and pitch angle trend vs. TSR.

model described in Eq. (13) the lift coefficient is increased in order to take into account the radial flow along the blades that provides an increase in energy with the same flow.

Fig. 11 shows a comparison between different simulation mathematical models (presented in [8]) and the model developed during our research. The model implemented in this work gives the best agreement between experimental and simulated data.

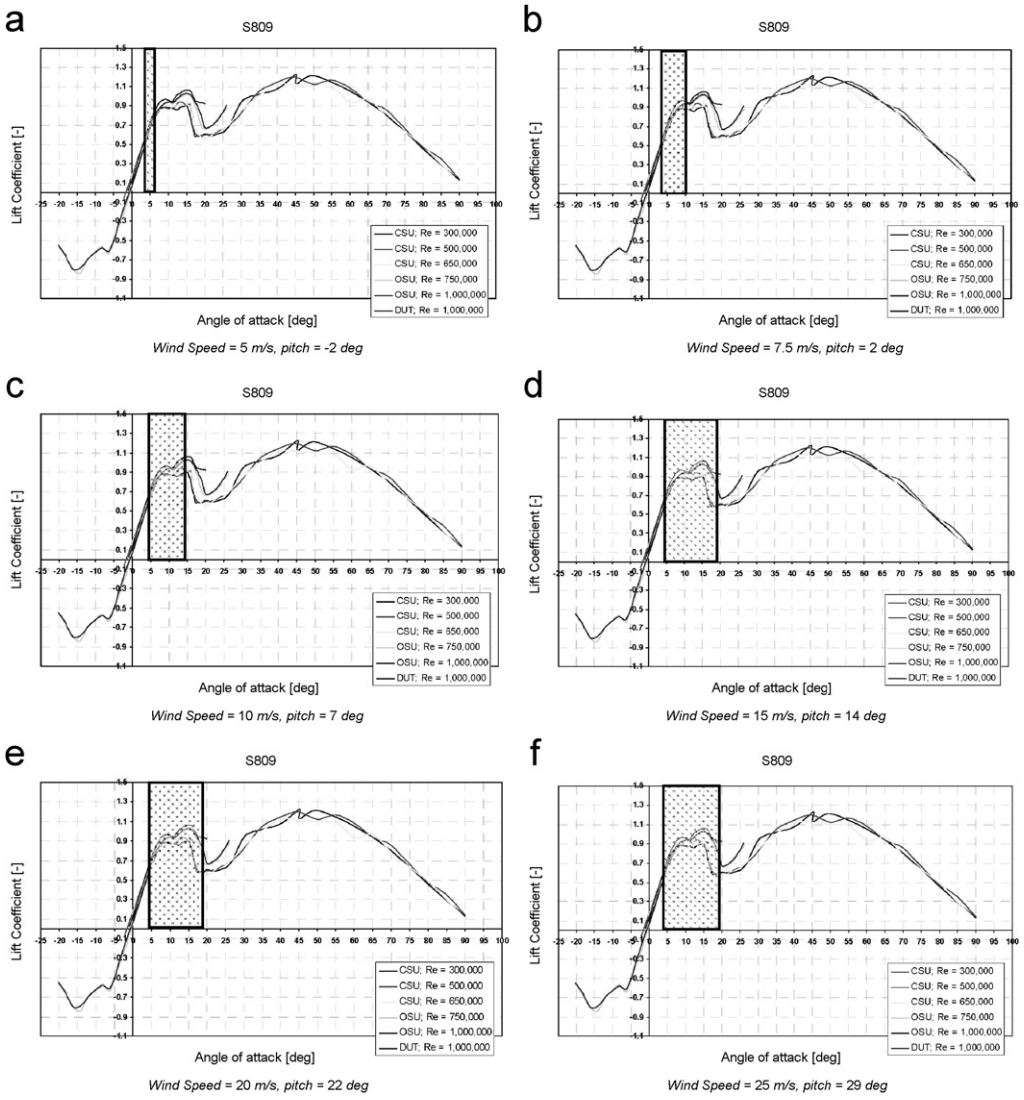

Fig. 14. Lift coefficient along the blade for the optimized wind rotor.

7. Wind turbine performance and power coefficient maximization

In fluid dynamics wind turbine design, maximization of the power coefficient C_P [19,20], (defined below), is of fundamental importance in order to maximize the extraction of energy from the wind.

$$C_P = \frac{P}{\frac{1}{2}\rho V_0^3 \pi R_1^2}. \tag{16}$$

Fig. 12 shows the experimental and simulated C_P (for a pitch angle of 3°). The experimental and simulated data (for a pitch angle of 3°) show a good agreement, and this

indicates that the mathematical model yields reliable results. So, as an example of optimization, the mathematical model was implemented to maximize the power coefficient for a wind turbine with a variable pitch angle at different wind velocities. By varying the pitch angle as represented in Fig. 12, it is possible to maximize the power coefficient, as indicated in the same figure by the curve labeled "Optimization (variable pitch with wind speed)". From Fig. 12 it is possible to notice that the wind turbine with a pitch angle of 3° is optimized for a wind speed of 8 m/s. Fig. 12 also shows the optimization of the power coefficient with other wind velocities. Of fundamental importance is the increase in the C_P value at low wind velocities (about 30%), in order to have a bigger torque; it represents a crucial point for the start of the wind rotor. Fig. 13 represents the same as in Fig. 12, but versus the TSR.

The changed flow conditions for the optimized rotor are represented in Fig. 14. On making a comparison between Figs. 9 and 14, it is possible to notice the difference in the distribution along the blade of the lift coefficient. At low wind velocities, the lift coefficient in Fig. 9 varies from 0.25 to 0.55, while for the optimized rotor the lift coefficient varies from 0.55 to 0.85. For both configurations the drag coefficient is always the same (see Fig. 4).

8. Conclusion

In this work a mathematical model for the fluid dynamics design of a wind turbine, based on Glauert theory, has been implemented. The mathematical model is known as the blade element momentum theory, and starts from the Glauert propeller theory, with suitable modifications for application to wind turbines. This model can be implemented for the study, design and evaluation of wind turbine rotor performance. The most difficult issues for the BEM theory are: mathematical representation of the correct lift and drag coefficient values and correct evaluation of the axial and tangential induction factors. On the basis of experimental measurements on a wind turbine, several simulations have been carried out to evaluate the best lift and drag coefficient representation, in order to take into account the effect of centrifugal pumping, and to better evaluate the influence of different induction factor representations.

Having chosen the representation for the aerodynamic coefficients and the induction factors, a comparison between the model implemented in this work and other mathematical models found in the literature was made. The comparison showed a good agreement between the model proposed in this work and experimental data.

After evaluation of the performance of the wind rotor, the mathematical model was implemented to optimize the power coefficient of the rotor, in order to maximize the torque available at low wind speeds.

References

[1] Meyer CJ, Kroger DG. Numerical simulation of the flow field in the vicinity of an Axial fan blade". Int J Num Methods Fluids 2001;36:947–69.
[2] Moriarty PJ, Hansen AC. AeroDyn theory manual. Technical report NREL/TP-500-36881—January 2005.
[3] Buhl Jr, L. A new empirical relationship between thrust coefficient and induction factor for the turbulent windmill state. Technical report NREL/TP-500-36834—August 2005.
[4] Glauert H. The analysis of experimental results in the windmill brake and vortex ring states of an airscrew. ARCR R&M 1926(1026).

[5] Jonkman JM. Modeling of the UAE Wind Turbine for refinement of FAST_AD. NREL/TP-500-34755, December 2003.
[6] Corten GP. Flow separation on wind turbine blades. PhD. thesis—Utrecht University, January 2001.
[7] Sphera DA, editor. Wind turbine technology: fundamental concepts of wind turbine engineering. 1998.
[8] Lindenburg C. Investigation into rotor blade aerodynamics. ECN-C-03-025, July 2003.
[9] Glauert H. The elements of airfoil and airscrew theory. Cambridge: Cambridge University Press; 1926.
[10] Hansen MOL. Documentation of code and airfoil data used for the NREL 10-m wind turbine. ROTABEM-DTU, November 2000.
[11] Duquette MM, Visser KD. Numerical implications of solidity and blade number on rotor performance of horizontal-axis wind turbine. J Sol Energy Eng—ASME 2003;125/425.
[12] Giguère P, Selig MS, Tangler JL. Blade design trade-offs using low-lift airfoil for stall-regulated HAWTs. J Sol Energy Eng—ASME 1999;121/217.
[13] Tangler JL. The evolution of rotor and blade design. NREL/CP-500-28410, July 2000.
[14] Wood D. The design and analysis of small wind turbine. University of Newcastle; 2002 notes.
[15] Maalawi KY, Badr MA. A practical approach for selecting optimum wind rotor. Renew Energy 2003;28: 803–22.
[16] Maalawi KY, Badawy MTS. A direct method for evaluating performance of horizontal axis wind turbines. Renew Sustain Energy Rev 2001;5:175–90.
[17] Varol A, Ilkilic C, Varol Y. Increasing the efficiency of wind turbines. J Wind Eng Ind Aerodyn 2001;89:809–15.
[18] Bermudez L, Velazquez A, Matesanz A. Viscous–inviscid method for the simulation of turbulent unsteady wind turbine airfoil flow. J Wind Eng Ind Aerodyn 2002;90:643–61.
[19] Maalawi KY, Negm HN. Optimal frequency design of wind turbine blades. J Wind Eng Ind Aerodyn 2002; 90:961–86.
[20] Giguère P, Selig MS. Design of a tapered and twisted blade for the NREL combined experiment rotor. NREL/SR-500-26173, April 1999.